iRGD peptide conjugation potentiates intraperitoneal tumor delivery of paclitaxel with polymersomes

Lorena Simón-Gracia[1]*, Hedi Hunt[1], Pablo Scodeller[1,2], Jens Gaitzsch[3,4], Venkata Ramana Kotamraju[2], Kazuki N. Sugahara[2,5], Olav Tammik[6], Erkki Ruoslahti[2,7], Giuseppe Battaglia[3], Tambet Teesalu[1,2,7]*.

[1]Laboratory of Cancer Biology, Institute of Biomedicine, Centre of Excellence for Translational Medicine, University of Tartu, Ravila 14b, 50411 Tartu, Estonia.

[2]Cancer Research Center, Sanford-Burnham-Prebys Medical Discovery Institute, 10901 North Torrey Pines Road, La Jolla, 92037 California, USA.

[3]Department of Chemistry, University College London, 20 Gordon Street. WC1H OAJ, London, UK.

[4]Department of Chemistry, University of Basel, Klingelbergstrasse 80, 4056 Basel, Switzerland.

[5]Department of Surgery, Columbia University College of Physicians and Surgeons, New York, New York, USA.

[6]Department of Surgical Oncology, Tartu University Hospital, Puusepa 8, 50411 Tartu, Estonia

[7]Center for Nanomedicine and Department of Cell, Molecular and Developmental Biology, University of California, Santa Barbara Santa Barbara, 93106 California, USA.

*Corresponding authors. Tambet Teesalu: Laboratory of Cancer Biology, Institute of Biomedicine, Centre of Excellence for Translational Medicine, University of Tartu, Ravila 14b, 50411 Tartu, Estonia. *E-mail address*: tteesalu@sbpdiscovery.org. Lorena Simon-Gracia: Laboratory of Cancer Biology, Institute of Biomedicine, Centre of Excellence for Translational Medicine, University of Tartu, Ravila 14b, 50411 Tartu, Estonia. *E-mail address*: Lorena.Simon.Gracia@ut.ee.

RUNNING TITLE: iRGD-polymersomes for IP tumor treatment

ABSTRACT

Polymersomes are versatile nanoscale vesicles that can be used for cytoplasmic delivery of payloads. Recently, we demonstrated that pH-sensitive polymersomes exhibit an intrinsic selectivity towards intraperitoneal tumor lesions. A tumor homing peptide, iRGD, harbors a cryptic C-end Rule (CendR) motif that is responsible for neuropilin-1 (NRP-1) binding and for triggering extravasation and tumor penetration of the peptide. iRGD functionalization increases tumor selectivity and therapeutic efficacy of systemic drug-loaded nanoparticles in many tumor models. Here we studied whether intraperitoneally administered paclitaxel-loaded iRGD-polymersomes show improved efficacy in the treatment of peritoneal carcinomatosis. First, we demonstrated that the pH-sensitive polymersomes functionalized with RPARPAR (a prototypic CendR peptide) or iRGD internalize in the cells that express NRP-1, and that internalized polymersomes release their cargo inside the cytosol. CendR-targeted polymersomes loaded with paclitaxel were more cytotoxic on NRP-1-positive cells than on NRP-1-negative cells. In mice bearing peritoneal tumors of gastric (MKN-45P) or colon (CT26) origin, intraperitoneally administered RPARPAR and iRGD-polymersomes showed higher tumor-selective accumulation and penetration than untargeted polymersomes. Finally, iRGD-polymersomes loaded with paclitaxel showed improved efficacy in peritoneal tumor growth inhibition and in suppression of local dissemination compared to the pristine paclitaxel-polymersomes or Abraxane.

Our study demonstrates that iRGD-functionalization improves efficacy of paclitaxel-polymersomes for intraperitoneal treatment of peritoneal carcinomatosis.

KEYWORDS: Polymersomes, tumor penetrating peptides, peritoneal carcinomatosis, paclitaxel, iRGD, NRP-1

INTRODUCTION

Gastrointestinal and gynecological cancers frequently spread in the peritoneal cavity resulting in disseminated tumors, condition known as peritoneal carcinomatosis (PC [1]). The prognosis of PC is grim; despite aggressive combination treatment that includes cytoreductive surgery and chemotherapy, the median survival is typically in the range of few months [2], [3], [4]. Optimal cytoreduction of the primary tumor can be achieved in 80% of patients with advanced ovarian cancer, and, to a lesser extent, in patients with gastrointestinal cancer [1]. However, microscopic tumor nodules and disseminated cancer cells that remain in the peritoneal cavity may give rise to new tumors and result in cancer recurrence [1]. Compared to the systemic route, intraperitoneal (IP) chemotherapy exposes the peritoneal tumors to elevated drug concentration with less systemic toxicity. IP therapy can be potentiated by increasing the temperature of the drug solution to improve penetration [2], [3], [4]. However, even in the hyperthermic IP chemotherapy, tumor penetration of anticancer drugs remains limited to the outer 2 mm [1], [4], [5]. Abdominal pain and toxicity due to the high local drug concentration in the peritoneal organs and tissues are important limitations of IP therapy [1]. Up to 60% of PC patients have recurrent disease [6], underlining the lack of effectiveness of the current treatments and the urgent need for improved treatment options.

Affinity ligands, such as peptides and antibodies that bind to tumor-associated markers, can be used to improve biodistribution and efficacy of anticancer drugs. We have discovered a new class of targeting peptides, tumor-penetrating peptides, that home to tumors and are actively transported into extravascular tumor parenchyma [7], [8]. Cell and tissue-penetration of this class of peptides requires the C-terminal exposure of the C-end rule (CendR) motif (consensus R/KXXR/K, R is arginine, K is lysine and X is any amino acid [9]. The CendR receptor, neuropilin-1 (NRP-1), is overexpressed in many tumor cell lines in vitro and in tumor and stromal cells in vivo [10]. The prototypic CendR peptide RPARPAR binds to NRP-1 and NRP-2 and triggers cellular internalization, extravasation, and tissue penetration of the peptide and payloads coupled to it [11], [12]. iRGD peptide (CRGDKGPDC) is a composite of the RGD αv-integrin-binding motif and an RGDK cryptic CendR motif. Once recruited to a tumor through the RGD motif, the CendR motif of iRGD is exposed through cleavage by a tumor-derived protease(s) and

triggers tumor-specific vascular exit and tissue penetration [13]. As processed iRGD interacts with NRP-1 in tumor vessels, a temporal increase in transcytosis takes place, and compounds co-administered with iRGD extravasate and accumulate in tumors [11], [13], [14], [15], [16], [17], [18], [19], [20], [21]. Relevant to current study, we recently demonstrate that iRGD increases targeting and antitumor activity of IP drugs that are co-administered with the peptide [14].

Polymersomes are nanoscale vesicles formed by self-assembly of amphiphilic block copolymers in aqueous media [22]. Polymersomes made of low glass transition temperature "rubbery" polymers are flexible and pass through pores up to an order of magnitude smaller than their diameter [23], [24], [25], [26]. The low surface area to membrane thickness ratio and its effect on surface tension, make polymersomes more flexible than smaller micelles, and therefore more able to deform to pass across narrow passages. The increased translocation ability of polymersomes can facilitate transport of drugs across biological barriers such as tumor tissue and blood vessels. Poly(oligoethylene glycol methacrylate)-poly(2-(diisopropylamino)ethyl methacrylate) ($P[(OEG)_{10}MA]_{20}$-$PDPA_{90}$; POEGMA-PDPA) polymersomes are pH-sensitive (Fig. S1): the particles are stable at physiological pH and disassemble under mildly acidic pH due to the protonation of the PDPA block [27], [28]. This property of POEGMA-PDPA vesicles renders them well suited for cellular cargo delivery: following cellular internalization, the polymersomes disassemble at endosomal acidic pH followed by endosomal rupture and release of cargo in the cytosol [29], [30], [31]. Thick and robust hydrophobic polymersome membrane is less leaky than lipid bilayer of liposomes [32]. We have demonstrated that the POEGMA-PDPA polymersomes retain the drug inside for several weeks at neutral pH and quickly release the cargo at mildly acidic pH [27]. pH-sensitive polymersomes have been used for intracellular delivery of DNA [29], antibodies [33], [34], [35], antibiotics [36], cytotoxic drugs [27], [37], [38], and peptides [39]. Systemic cargo delivery with polymersomes in solid tumors in mice as well as tumor imaging has been potentiated by affinity targeting with ligands such as RGD peptide [40], PR_b-peptide [41], or transferrin [42], [43].

Recently, we demonstrated in PC models that IP paclitaxel (PTX)-loaded POEGMA-PDPA polymersomes have superior anticancer activity compared to the free drug or albumin-PTX nanoparticles, Abraxane®

(ABX) [27]. Here we set out to determine whether affinity targeting of IP administered PTX-polymersomes with tumor penetrating peptides improves their tumor selectivity and therapeutic efficacy. We demonstrate that RPAR and iRGD peptides deliver polymersomes to their target molecules and that IP-administered targeted polymersomes loaded with PTX are more efficacious than untargeted polymersomes.

MATERIALS AND METHODS

Materials

$CHCl_3$, MeOH, dimethylformamide (DMF), rhodamine B octadecyl ester, doxorubicin, and paclitaxel were purchased from Sigma-Aldrich, Germany. Phosphate-buffered saline (PBS) was purchased from Lonza, Belgium. MKN-45P human gastric cancer cells were isolated from parental MKN-45 cells [44]. CT26 cell line (CT.26 ATCC CLR-2638) was purchased from ATCC. PPC-1 cells were from the Ruoslahti laboratory at Sanford-Burnham-Prebys Medical Discovery Institute (SBPMDI) and M21 cells were a gift from David Cheresh at University of California San Diego (UCSD). The cells were cultivated in DMEM (Lonza, Belgium) containing 100 IU/mL of penicillin, streptomycin, and 10% of heat-inactivated fetal bovine serum (GE Healthcare, UK). Athymic nude mice were purchased from HSD, and Balb/c mice were purchased from Charles River. iRGD peptide with an extra cysteine residue for NP coupling was synthesized at SBPMDI and RPARPAR peptide was purchased from TAG Copenhagen (Denmark). All the animal experimentation protocols were approved by Estonian Ministry of Agriculture, Committee of Animal Experimentation (Project #42).

POEGMA-PDPA copolymer synthesis

The 4-(2-bromoisobutyryl ethyl) morpholine initiator (MEBr) was prepared according to a previously published procedure [45]. The protected maleimide initiator (Mal-Br) was prepared according to a previously published procedure [46]. ATRP synthesis and purification of $P(OEG_{10}MA)_{20}$-$PDPA_{90}$ from ME-Br, Rho-Br and Mal-Br initiators was carried out as previously described [35], [47]. The copolymer composition was analysed by 1H NMR in $CDCl_3$ and the polydispersity was determined by size exclusion chromatography in acidic water (0.25 vol% TFA in water). The deprotection of Mal-$P(OEG_{10}MA)_{20}$-$PDPA_{90}$ was carried out according to a previously described procedure [35].

Reaction of Mal-$P(OEG_{10}MA)_{20}$-$PDPA_{90}$ with cysteine-terminated peptides and 5(6)-carboxyfluorescein (FAM)

The deprotected Mal-P($OEG_{10}MA)_{20}$-$PDPA_{90}$ (20 mg, 0.7 μmol) was dissolved in 1 mL of $CHCl_3$:MeOH 2:1, and 2 eq of Cys-peptides or Cys-FAM dissolved in 1 mL of nitrogen-purged DMF, were added to the solution. The mixture was stirred at 300 rpm overnight at RT. $CHCl_3$ and MeOH were evaporated, and the remaining solution was dialyzed against water using a dialysis cassette (Thermo Scientific, USA) with a molecular weight cut-off of 10 KDa to remove the excess of Cys-peptides or Cys-FAM. The resulting suspension was freeze-dried and a yellow powder was obtained.

Polymersome formation and loading with paclitaxel, rhodamine B octadecyl ester, and doxorubicin (DOX)

To generate FAM-labeled polymersomes (FAM-PS), FAM-labeled RPARPAR-polymersomes (R-FAM-PS), or FAM-labeled iRGD-polymersomes (iRGD-FAM-PS), FAM-P($OEG_{10}MA)_{20}$-$PDPA_{90}$ or FAM-peptide-P($OEG_{10}MA)_{20}$-$PDPA_{90}$ was mixed with the non-labeled copolymer at a ratio of 1:4. For the formation of polymersomes and encapsulation of PTX or DOX, 20 mg of copolymer were dissolved in 4 mL of $CHCl_3$:MeOH 2:1 in a glass vial, and 100 μL of PTX or DOX dissolved in MeOH at a concentration of 5 mM were added to the copolymer solution (0.25 mM PTX or DOX/mL as a final concentration). For the encapsulation of rhodamine B octadecyl ester, 20 mg of copolymer was dissolved in 4 mL of $CHCl_3$:MeOH 2:1 in a glass vial, and 50 μL of rhodamine B dissolved in $CHCl_3$:MeOH at 1 mg/mL were added. The solution was dried under vacuum to allow for the formation of the polymer film. The films were hydrated with 2 mL of PBS (pH 7.4) and stirred at 300 rpm for 2 weeks. Next, the suspension was sonicated for 30 min at RT and the polymersomes were purified by centrifugation (500 g for 20 minutes at RT, followed by centrifugation of the supernatant at 20,000 g for 20 min at RT). The pellet was resuspended in 2 mL of PBS (pH 7.4). The yield of polymersomes formed by film hydration was determined by weighing the solid residue after lyophilization of polymersome suspension in water. The amount of FAM-labeled targeting peptides in polymersomes was quantified by fluorometry (FlexStation II, Molecular Devices) at 485/520 nm.

Dynamic Light Scattering (DLS) and Z-potential measurements (Zetasizer Nano ZS, Malvern Instruments) was used to assess the polydispersity and average size of polymersome preparations in a

different pH buffers, and their surface charge. Transmission electron microscopy (TEM) was used to assess the size, surface topology and morphology of assembled vesicles. TEM of phosphotungstic acid stained polymersomes was used to visualize the polymersome surface topology and structure [48], [49]. Briefly, polymersomes in PBS at pH 7.4 or at pH 5.5 were deposited onto copper grids at 1 mg/mL, stained with 0.75% phosphotungstic acid (pH 7), air-dried, and imaged by TEM (Tecnai 10, Philips, Netherlands). Polymersome-encapsulated PTX was quantified by ultra-performance liquid chromatography (UPLC, Waters), using free PTX dissolved in MeOH to prepare the standard curve. Fifty µL of PTX-polymersomes were mixed with 50 µL of MeOH and 2 µL of HCl 1M. 5 uL of this mixture was run using water/ACN as eluent and Acquity Ultraperformance UPLC BEH C18 1.7 uM 2.1x50 mm column.

In vitro cytotoxicity assay

Cytotoxicity experiments were performed using the xCELLigence® RTCA DP instrument (Roche Diagnostics, GmbH, Mannheim, Germany and ACEA Biosciences, Inc. San Diego, CA, USA). Experiments were carried out using disposable 16-well xCELLigence® E-Plates with microelectrodes attached to the bottom of the wells for impedance measurement. Initially, 50 uL of complete medium was added to the wells and background impedance was measured for each well. Subsequently, 50 uL of complete medium containing 10^5 cells was added to each well and E-plates were incubated in the RTCA DP device at 37° C for 24 hours. The impedance value was automatically monitored every 30 minutes and expressed as a cell index value (CI). Twenty-four hours after cell seeding, polymersomes were added in triplicate at a final concentration of 100 nM of PTX. Complete medium alone was added to the control wells. CI was determined every 30 minutes over the following 25 hours. All data was recorded using RTCA software version 1.2.1. CI-data from the experiments was normalized to the last data point prior to the addition of compounds. The data was expressed as % viability compared to the untreated cells.

Evaluation of cellular uptake and cargo release

PPC-1, M21, MKN-45P, or CT26 cells ($5x10^5$ cells) were seeded on glass coverslips in a 24-well plate. After 24 hours, polymersomes were added to the cells at a concentration of 0.5 mg/mL and incubated for 1 hour or 24 hours. The cells were washed with PBS, fixed with 4% of paraformaldehyde in PBS, inmunostained with rabbit NRP-1 antibody (Abcam, UK) and Alexa 647-conjugated goat anti-rabbit IgG antibody (Invitrogen, USA), stained with DAPI, and imaged with fluorescence confocal microscopy (Zeiss LSM 510). The images were processed and analyzed using the ZEN lite 2012 image software.

In vitro binding of polymersomes to recombinant proteins

His-tagged NRP-1 b1b2 domain and p32 were expressed and purified as described [9], [50]. Ni-NTA magnetic agarose beads (Qiagen) in Tris buffer (50 mM Tris pH 7.4, 150 mM NaCl, 0.05% NP40, 5 mM imidazole) were loaded with either the b1b2 binding domain of NRP1 or with p32 protein (at 10 μg of protein/μg beads). Rho-labeled polymersomes were incubated for one hour with the protein-loaded beads in Tris buffer with 1% BSA at RT with gentle mixing, followed by washes, and release with high-imidazole buffer (PBS, 400 mM imidazole, 150 mM NaCl, 1% BSA, 0.05% NP40). The fluorescence of eluted samples was quantified with a fluorescence plate reader (FlexStation II, Molecular Devices equipment).

In vivo biodistribution studies

Nude mice were injected IP with $2x10^6$ MKN-45P cells and subcutaneously (SC) in the right flank with 10^6 MKN-45P cells. Balb/c mice received IP injection of $2x10^6$ CT26 cells and SC inoculation of $0.5x10^6$ CT26 cells. The MKN-45P tumors were grown for two weeks and the CT26 tumors for one week. FAM-labeled polymersomes were injected IP (0.5 mg in 500 μL of PBS) or IV (0.5 mg in 100 μL of PBS) and 4 hours later the animals were perfused with 10 mL of PBS. The tumors and organs were excised for the fluorescence visualization using Illumatool (Lightools Research, USA) and the fluorescence quantification by Image J software. Tissues were snap-frozen in liquid nitrogen, and stored at -80°C for further analysis.

Immunofluorescence and microscopic imaging

The excised tumors and organs were cryosectioned at 10 μm, fixed with 4% of paraformaldehyde in PBS, and immunostained with rabbit anti-fluorescein (Life Technologies, USA) and rat anti-mouse CD31 (BD Biosciences, USA) as primary antibodies, and with Alexa 488-conjugated goat anti-rabbit IgG and Alexa 647-conjugated goat anti-rat IgG (Invitrogen, USA) as secondary antibodies. Alternatively, the tissue sections were immunostained with rabbit anti-NRP-1 (Abcam, UK) or rabbit anti-αv-integrin (Millipore, US) followed by Alexa 647-conjugated goat anti-rabbit IgG (Invitrogen, USA). The nuclei of cells were stained with 10μg/ml DAPI. Confocal images of the tissue sections were analyzed with the ZEN lite 2012 image software.

Ex vivo tumor dipping assay.

Fresh surgical samples of peritoneal metastases of colon cancer were collected under protocols approved by the Ethics Committee of the University of Tartu, Estonia (permit #243/T27). The samples were immediately divided in explants of around 1 cm^3 and incubated in DMEM containing 1% of BSA and 0.5 mg/mL of iRGD-FAM-PS or FAM-PS at 37°C for 4 hours. After 3 washes with PBS, the tumors were cryosectioned and stained for rabbit anti-fluorescein antibody followed by Alexa 546-conjugated anti-rabbit antibody.

Experimental tumor therapy in mice

For the MKN-45P treatment study, the athymic nude mice were injected IP with 2 x10^6 MKN-45P cells. Three days after the cell injection, the mice were randomized in 4 groups (n = 8). The mice were treated every other day with IP injections of 0.5 mL of ABX, PS-PTX, or iRGD-PS-PTX, at the same PTX dose (cumulative dose: 7 mg/Kg). Different solvents (salt-based, dextrose-based, hetastarch, or icodextrin) have been used for chemotherapeutics during IP chemotherapy [1]. We administered all the compounds in phosphate buffered saline (PBS) that we used to form the polymersomes and to dissolve ABX for in vivo treatment studies in the past [51]. After 18 days of tumor induction the mice were perfused with 10 mL of

PBS and the tumors and organs were excised. To estimate the tumor burden, the total weight of large (tumors bigger than 5 mm in diameter) and medium peritoneal tumors (tumors bigger than 2 mm and smaller than 5 mm of diameter) together with the small metastatic peritoneal nodules (tumor nodules smaller than 2 mm of diameter) was determined. To assess the extent of tumor dissemination, the individual peritoneal nodules were counted. In CT26 treatment study, dual tumor mice were used: Balb/c mice were injected with IP with $0.5x10^6$ and SC with $0.5x10^6$ CT26 cells. Four days after tumor induction, the volume of s.c. tumors was determined with a caliper (formula: width x height x depth) and the animals were distributed in 5 groups (n = 4) with the same average of s.c. tumor volume. The mice were treated every other day with IP injections of 0.5 mL of ABX, PS-PTX, iRGD-PS-PTX (cumulative dose of PTX: 4.5 mg/Kg), empty PS, or PBS. After 12 days of tumor induction animals were perfused with 10 mL of PBS, the ascites volume was measured, and peritoneal and s.c. tumors were weighed.

Statistical analysis

Student's *t*-test or one-way analysis of variance (ANOVA) and Fisher LSD was performed with StatSoft Statistica 8 software.

RESULTS

Assembly and characterization of polymersomes

The polymersomes were assembled and loaded with PTX using the hydration film method [37]. The yield of polymersomes was 40±6% and the drug loading was 1.4±0.2 moles of PTX/mol polymer (~ 10^5 drug molecules per vesicle). Polymersomes were functionalized with $1.6x10^3$ peptide/polymersome (~$1.1x10^2$ peptides/nm^2), close to estimated optimal density of affinity ligands for nanoparticle targeting [52] and in the same range of the density of displayed peptides on the coat of T7 bacteriophage used to identify the targeting peptides (~200 peptides/60 nm T7 particle, ~$1.7\ x10^2$ peptides/nm^2) [53]. The average polymersome size was 214 nm (Pdi 0.16) for PTX-loaded polymersomes (PS-PTX), 228 nm (Pdi 0.12) for PTX-loaded RPARPAR-polymersomes (R-PS-PTX), and 233 nm (Pdi 0.17) for PTX-loaded iRGD-polymersomes (iRGD-PS-PTX) (Fig. S2). The Z-potential was slightly negative for PS-PTX and iRGD-PS-PTX (-3.6±0.4 and -2.7±0.1 mV respectively) and neutral for R-PS-PTX (+0.15±0.3) (Fig. S3). The size and Z-potential remains virtually unchanged for the targeted and non-targeted polymersomes, indicating that the differences in cellular uptake and tumor penetration are consequence of the peptide-receptor interaction, but not of the morphology and surface charge effect.

The effect of pH modulation on polymersomes was assessed by determining their size at different pH values by DLS. Whereas the size of polymersomes at pH 7.4 was 214 nm (Pdi 0.16), at lower pH increase in polydispersity (Pdi 0.65 at pH 5.5 and Pdi 0.62 at pH 4.5) and in size was observed (Fig. S4). By TEM formation of polymer aggregates and disappearance of vesicle-like structures at pH 5.5 was seen (Fig. S4), in line with destabilization and disassembly of the polymersomes under acidic conditions.

CendR peptides modulate polymersome tropism in vitro

To study the specific binding and internalization of polymersomes conjugated with CendR peptides in cultured cells, we used PPC-1 human prostate cancer cells, which express high levels of NRP-1, and M21 human melanoma cells, which are NRP-1-negative [9], [20]. The NRP-1 expression status of PPC-1 and M21 cells was confirmed by confocal microscopy (Fig. 1A and 1B) and by flow cytometry (Fig. S6).

Fluorescein-labeled RPARPAR-polymersomes (R-FAM-PS) bound to and internalized in PPC-1 cells within 1 hour, whereas no fluorescence was observed in M21 cells (Fig. 1A). Fluorescein-labeled iRGD-polymersomes (iRGD-FAM-PS) also preferentially targeted PPC-1cells (Fig.1A). However, the uptake was lower than that of R-FAM-PS, likely because iRGD first binds to αv-integrin and acquires NRP-binding ability only after the proteolytic cleavage step that exposes its CendR motif, whereas the RPARPAR binds to NRP-1 directly and, therefore, faster [12]. No uptake of fluorescein-labeled untargeted polymersomes (FAM-PS) on PPC-1 was observed after one hour of incubation (Fig. 1A). At 24 hours of incubation, increased cellular accumulation of iRGD-FAM-PS was seen, with similar uptake to that observed for R-FAM-PS (Fig S7). At 24 hours, a low-level background uptake of untargeted polymersomes was seen in both PPC-1 and M21 cells, possibly due to the constitutive endocytosis of polymersomes (Fig S7). These experiments show that CendR peptides can be used to target polymersomes to NRP-1-expressing cultured cells.

To confirm the specific interaction of CendR-polymersomes to NRP-1, we also tested the binding in a cell-free system. RPARPAR-polymersomes (R-PS) readily bound to immobilized recombinant b1b2 domain of NRP-1 (Fig. 1B). The R-PS showed only background binding to recombinant p32 (a control protein, known to bind to non-CendR basic peptides; [50]) and untargeted polymersomes did not bind to either protein. These data show that homing peptides coated on the polymersomes are available for receptor interactions and that the tropism of polymersomes can be specifically modulated by functionalization with CendR peptides.

CendR-targeted polymersomes release their cargo in the cytosol

Polymersomes containing PDPA polymeric block are well-suited for cytoplasmic cargo delivery: following cellular uptake the polymersomes break down, trigger endosomal rupture and release their cargo into the cytosol [29], [30], [31]. We used PPC-1 cells to study if the endosomal escape pathway remains operational in polymersomes internalized via the CendR pathway. Rhodamine B octadecyl ester (Rho) or DOX was encapsulated in R-FAM-PS and in FAM-PS. After 1-hour incubation of PPC-1 cells with R-FAM-PS loaded with Rho, widespread Rho fluorescence was observed in the cytoplasm (Fig. 1C).

Interestingly, already 1 hour after incubation with the cells, the R-FAM-polymer and Rho cargo exhibited clearly different intracellular distribution patterns (Fig. 1C, arrow). After 1-hour incubation of PPC-1 cells with the DOX-loaded R-PS, the red DOX fluorescence was observed in the nuclei of the cells (Fig. 1D, arrow). In contrast, only a weak DOX signal was seen in PPC-1 cells incubated in the presence of DOX-loaded untargeted polymersomes (Fig. 1D). These data suggest that cellular uptake of CendR-polymersomes is followed by disassembly of polymersomes and cytosolic release of the payloads.

In vitro cytotoxicity of targeted PTX-polymersomes

We next studied whether CendR polymersomes can be used to potentiate in vitro cytotoxicity of PTX. As a reference, we used ABX, a colloidal suspension of paclitaxel and human serum albumin that is clinically approved for the treatment of several types of solid tumors (breast, lung, pancreatic, and gastric carcinoma), and is in advanced clinical trials for the treatment of colorectal cancer. We studied the viability of PPC-1 and M21 cells exposed to polymersomes and ABX (all at 100 nM PTX). In PPC-1 cells, R-PS-PTX and iRGD-PS-PTX were significantly more toxic than PS-PTX, or ABX (Fig. 2 and Fig. S8A). In agreement with the cellular uptake data, the R-PS-PTX and iRGD-PS-PTX had a similar cytotoxic effect on PPC-1 cells at 24 hours (Fig. S7). About 50% of PPC-1 cells treated with R-PS-PTX or iRGD-PS-PTX remained viable after 24 hours of incubation, whereas about 80% of cells treated with PS-PTX were viable, and ABX had only a negligible effect (Fig. 2 and Fig. S8A). In contrast to NRP-1-positive PPC-1 cells, the viability of M21 was not significantly affected after 24-hour exposure to R-PS-PTX or iRGD-PS-PTX (Fig. 2 and Fig. S8B). Empty polymersomes had no effect on cell viability in all the cell lines and time points tested. These experiments show that PTX-polymersomes targeted with CendR-peptides specifically decrease the viability of cultured NRP-1-expressing cells.

IP-administered CendR polymersomes home to peritoneal and subcutaneous tumors

We next studied tumor homing of IP administered polymersomes to peritoneal and subcutaneous MKN-45P and CT26 tumors in mice. MKN-45P is a human gastric cancer cell line with a high potential for peritoneal dissemination [44]. CT26 mouse colon carcinoma cell line can be used for modeling PC in syngeneic immunocompetent mice [27]. We first evaluated binding and uptake of R-FAM-PS, iRGD-

FAM-PS, and FAM-PS in MKN-45P and CT26 in cultured cells. Although the expression of NRP-1 in MKN-45P and CT26 cells was lower than in PPC-1 cells, their profile of uptake of targeted polymersomes was comparable to PPC-1 cells (Fig. S9). After 1 hour of incubation, the internalization of R-FAM-PS was the highest and the uptake of control FAM-PS was low in both cell lines. At 24 hours, we observed similar uptake of R-FAM-PS and iRGD-FAM-PS in both MKN-45P and CT26 cells, whereas FAM-PS showed a weak signal (Fig. S9).

MKN-45P and CT26 cells implanted IP into mice gave rise to aggressive PC with the malignant tissue expressing high levels of NRP-1 (Fig. S10A) and αv-integrins (primary receptor of iRGD peptide, Fig. S10B). Macroscopic imaging of tissues after 4 hours of IP injection showed that R-FAM-PS and iRGD-FAM-PS accumulated in both MKN-45P and CT26 peritoneal tumors, but not in control organs, whereas FAM-PS gave a weaker tumor signal (Fig. 3A and 3B). The iRGD-FAM-PS group showed the highest fluorescence in IP tumors and only background signal was seen in control organs (Fig. 3C and 3D).

To obtain information on the microscopic distribution of the polymersomes, we immunostained the tissue sections with anti-FAM antibody. In agreement with the ex vivo macroscopic imaging, iRGD-FAM-PS showed the highest homing and penetration in both tumor models (Fig. 4A and 4C). In peritoneal and s.c. MKN-45P tumors, iRGD-FAM-PS were accumulated in the peritoneal tumor periphery and deep within the tumor mass (Fig. 4A and 4B, arrows), partially co-localizing with αv-integrins, NRP-1 (Fig. S6A), and CD-31-positive blood vessels (Fig. 4A and 4B, arrows).

The co-localization of iRGD-FAM-PS and blood vessels suggests that the accumulation in MKN-45P tumors takes place by a direct penetration from the peritoneal cavity and indirectly accumulation through systemic circulation. Although the accumulation of iRGD-FAM-PS in peritoneal CT26 tumors was also high, there was no co-localization with blood vessels (Fig. 4C), suggesting that the penetration in CT26 tumors was only locoregional.

We observed that IP-administered iRGD-FAM-PS homed to s.c. MKN-45P tumors better than to s.c. CT26 tumors (Fig. 4D and Fig. S12). This correlated with higher expression of NRP-1in s.c. MKN-45P tumors (Fig. S10B and S12B) compared to s.c. CT-26 tumors. In MKN-45P tumors, R-FAM-PS co-localized partially with CD31-positive blood vessels, although the accumulation and tumor penetration

was lower than for iRGD-FAM-PS (Fig. 4A). The RGD motif mediates recruitment to αv-integrins on tumor endothelial cells, fibroblasts and tumor cells; a proteolytic cleavage by a tumor–derived protease then exposes a NRP-1-binding tumor penetrating motif. The multi-step homing and tumor penetration pathway used by iRGD renders it highly selective towards malignant tissues positive for both αv-integrins and NRP-1[13]. In both tumor models, FAM-PS only weakly labeled the surface of the peritoneal tumors (Fig. 4A, arrowheads). These data indicate that iRGD-functionalization improves the accumulation of IP-administered polymersomes in IP tumors, and to some extent also in s.c. tumors.

To investigate the translational relevance of the iRGD-PS we evaluated the penetration of polymersomes into freshly excised human colon cancer PC lesions. iRGD-FAM-PS penetrated deeper and showed higher fluorescence in the clinical tumor samples than non-targeted polymersomes (Fig. S13). These data suggest that the polymersome nanocarriers targeted via the iRGD-pathway are potentially relevant for targeting of clinical PC lesions.

iRGD-functionalization enhances therapeutic efficacy of PTX-polymersomes

Having established preferential accumulation of iRGD-FAM-PS in cultured cancer cells and in peritoneal cancer lesions ex vivo and in vivo, we evaluated the therapeutic efficacy of iRGD-PS-PTX. Mice bearing disseminated MKN-45P IP tumors were treated with iRGD-PS-PTX, PS-PTX, or ABX, all at the cumulative PTX dose of 7 mg/kg. Among the formulations used, iRGD-PS-PTX gave the strongest antitumor response. The total weight of detectable peritoneal tumors treated with iRGD-PS-PTX was significantly lower than those in the ABX and untreated groups (Fig. 5). Importantly, treatment with iRGD-PS-PTX significantly reduced the number of peritoneal tumor nodules compared to the other treatments (Fig. 5).

In the CT26 model, treatment with both iRGD-PS-PTX and PS-PTX resulted in significantly reduced peritoneal tumor growth compared to the other groups, with iRGD-PS-PTX being the most efficient treatment (Fig. S14A). iRGD-PS-PTX had also an effect on s.c. CT26 tumors, although the difference was not significant (Fig. S14B). The total tumor burden (total weight of detectable peritoneal tumors and

s.c. tumors) was reduced by iRGD-PS-PTX in the CT26 model, and the reduction was significantly greater than that in the ABX and untreated groups, (Fig. S14C). One of the characteristics of the CT26 colon tumor model is accumulation of abundant ascites fluid in the peritoneal cavity. The ascites volume in CT26-bearing mice treated with iRGD-PS-PTX and PS-PTX was significantly lower than in other groups (Fig. S14D). These data show that iRGD functionalization potentiates the antitumor activity of IP-administered PTX-polymersomes in mouse models of PC and in extraperitoneal tumors, and that it may have a significant reducing effect on the tumor dissemination in the peritoneal cavity.

DISCUSSION

Nanoscale vesicles assembled from amphiphilic block copolymers are promising for applications that include surface functionalization and drug delivery. Our study was designed to evaluate if functionalization of pH-sensitive POEGMA-PDPA polymersomes with tumor-penetrating CendR peptides improves the utility of the polymersome platform for the treatment of PC. We found that CendR peptide RPARPAR is capable of recruiting polymersomes to recombinant NRP-1 and targeting them to NRP-1 positive cells. We also found that PTX-polymersomes targeted with CendR peptides are selectively cytotoxic to NRP-1-positive cells in vitro. Furthermore, our data demonstrate that IP-administered iRGD-PS accumulate in the malignant lesions in two mouse models of PC and in clinical tumor samples, and that IP iRGD-PS-PTX have an antitumor activity superior to PS-PTX or ABX. Thus,

CendR peptide-targeted polymersomes represent a promising preclinical development lead for IP delivery of cytotoxic drugs to PC lesions.

PTX is a potent chemotherapeutic compound that has shown efficacy for IP therapy of PC [54]. Because of low solubility in aqueous solutions, PTX is typically administered with Cremophor EL as a solvent, which is responsible for much of the clinical toxicity. Polymersomes made from amphiphilic copolymers can be loaded with hydrophobic drugs (in the membrane) and hydrophilic drugs (inside the aqueous lumen) to improve bioavailability and to sidestep the use of toxic solvents. Although here we only encapsulate a hydrophobic drug, the demonstration of the efficacy of targeted polymersomes for PC treatment opens directions for the development of multidrug-loaded polymersomes for an improved tumor therapy [38].

Recently, we showed that IP treatment of PC with PTX-loaded POEGMA-PDPA polymersomes resulted in better antitumor response than treatment with PTX-Cremophor EL and ABX [27]. The peritoneal space in patients with invasive gastric cancer has pH 7.4 or higher [55] - well above the pH that triggers the disassembly of polymersomes and their cargo release. During IP chemotherapy, slow drug release in the peritoneal cavity allows higher MTD (maximum tolerated dose) but is thought to drive drug resistance in the tumors. The effect of cytotoxic drugs is generally improved when the drug release is fast, supposedly due to the higher bioavailable peak drug concentration [1], [56], [57]. We have shown that whereas PTX is retained in polymersomes for months at physiological pH, polymersomes rapidly disassemble to release drug, after cellular internalization [27]. The fast release of PTX from internalized iRGD-PS may contribute to their efficacy in IP chemotherapy.

In a previous study we found that, for PC, IP-administered polymersomes were more tumor-selective than IV-administered polymersomes, which resulted in less accumulation in peritoneal tumors and more accumulation in the rest of body [27]. As shown in the current report, tumor accumulation of the polymersomes can be further improved by targeting with CendR peptides. A likely reason is that the iRGD-PS both homed to and penetrated through peritoneal tumors, whereas untargeted polymersomes accumulated only in the tumor periphery.

Tumor penetration of iRGD peptide is the result of a multistep mechanism that involves bindings to αv-integrins, proteolytic cleavage to expose the CendR motif of the peptide at the C-terminus, and binding of CendR motif to NRP-1, which then triggers a cell and tissue penetration cascade [13]. In line with this concept, we found that iRGD-polymersomes co-localized with the αv-integrins and NRP-1.

IP injected iRGD-PS accumulated in IP tumors and, to some extent, s.c. tumors, suggesting a mechanism that involves a combination of direct penetration and circulation-mediated homing. Such dual pathway allows payload delivery to both small avascular nodules and to large vascular tumors. This is an important advantage, as a number of clinical studies on PC indicate that combining systemic and IP chemotherapy results in better outcome than either route alone [58].

iRGD peptide is known to induce a tumor-specific temporal increase of transcytosis [11], [13]. As a result, iRGD-functionalized therapeutic compounds accumulate in the tumor and have improved therapeutic index [11]. We demonstrated that the iRGD further potentiates the activity of PTX-PS in a very low drug dose, suggesting that iRGD-PS loaded with cytotoxic drugs may be used to decrease side effects, increase efficacy, or achieve balance of both.

From the clinical perspective, local dissemination and micro-metastasis of PC poses a particular challenge: whereas the big peritoneal tumors can be surgically removed prior to the chemotherapy, microscopic metastatic nodules remain in the peritoneal cavity following surgical intervention. Peritoneal spread is particularly problematic for the successful treatment of gastric cancer. In patients with gastric cancer, 60% of deaths are associated with PC. Between 5-20% of gastric cancer patients who supposedly have “localized” tumor and potentially curative tumor resection are found to have PC, and after the resection the recurrence rate for PC is around 30% [1]. Importantly, we observed a significant decrease in IP MKN-45P tumor nodules in mice treated with iRGD-PS-PTX.

Finally, our studies on human colon PC explants, which show that iRGD-PS bind to and penetrate clinical tumors, serve as a starting point towards translation of the platform into clinical applications.

CONCLUSIONS

iRGD functionalization potentiates tumor selectivity and antitumor activity of IP PTX-loaded pH-sensitive POEGMA-PDPA polymersomes. In mouse models of PC and extraperitoneal tumors, iRGD-PS-PTX exhibited higher antitumor efficacy than untargeted polymersomes. These observations warrant future preclinical and clinical research aimed at the development of polymersome-based drug delivery systems for the treatment of PC.

ACKNOWLEDGMENTS

The authors thank Rein Laiverik (Department of Anatomy, University of Tartu) for the assistance with the TEM equipment in this work.

REFERENCES

[1] Intraperitoneal Cancer Therapy: Principles and Practice - CRC Press Book, (n.d.). https://www.crcpress.com/Intraperitoneal-Cancer-Therapy-Principles-and-Practice/Ceelen-Levine/9781482261189 (accessed April 24, 2016).

[2] G. Montori, F. Coccolini, M. Ceresoli, F. Catena, N. Colaianni, E. Poletti, L. Ansaloni, The treatment of peritoneal carcinomatosis in advanced gastric cancer: State of the art, Int. J. Surg. Oncol. 2014 (2014). doi:10.1155/2014/912418.

[3] Y.L.B. Klaver, V.E.P.P. Lemmens, S.W. Nienhuijs, M.D.P. Luyer, I.H.J.T. de Hingh, Peritoneal carcinomatosis of colorectal origin: Incidence, prognosis and treatment options., World J. Gastroenterol. 18 (2012) 5489–94. doi:10.3748/wjg.v18.i39.5489.

[4] R.N. Eskander, Cytoreductive surgery and hyperthermic intraperitoneal chemotherapy in epithelial ovarian cancer: State of the art, World J. Obstet. Gynecol. 2 (2013) 94. doi:10.5317/wjog.v2.i4.94.

[5] M. Tsai, Z. Lu, J. Wang, T.-K. Yeh, M.G. Wientjes, J.L.-S. Au, Effects of carrier on disposition and antitumor activity of intraperitoneal Paclitaxel., Pharm. Res. 24 (2007) 1691–701. doi:10.1007/s11095-007-9298-0.

[6] I. Königsrainer, P. Horvath, F. Struller, V. Forkl, A. Königsrainer, S. Beckert, Risk factors for recurrence following complete cytoreductive surgery and HIPEC in colorectal cancer-derived peritoneal surface malignancies., Langenbeck's Arch. Surg. / Dtsch. Gesellschaft Für Chir. 398 (2013) 745–9. doi:10.1007/s00423-013-1065-6.

[7] T. Teesalu, K.N. Sugahara, E. Ruoslahti, Tumor-penetrating peptides., Front. Oncol. 3 (2013) 216. doi:10.3389/fonc.2013.00216.

[8] E. Ruoslahti, Tumor Penetrating Peptides for Improved Drug Delivery., Adv. Drug Deliv. Rev. (2016). doi:10.1016/j.addr.2016.03.008.

[9] T. Teesalu, K.N. Sugahara, V.R. Kotamraju, E. Ruoslahti, C-end rule peptides mediate neuropilin-1-dependent cell, vascular, and tissue penetration., Proc. Natl. Acad. Sci. U. S. A. 106 (2009) 16157–16162. doi:10.1073/pnas.0908201106.

[10] J. Rieger, W. Wick, M. Weller, Human malignant glioma cells express semaphorins and their receptors, neuropilins and plexins., Glia. 42 (2003) 379–89. doi:10.1002/glia.10210.

[11] K.N. Sugahara, T. Teesalu, P.P. Karmali, V.R. Kotamraju, L. Agemy, D.R. Greenwald, E. Ruoslahti, Coadministration of a Tumor-Penetrating Peptide Enhances the Efficacy of Cancer Drugs, Science (80-.). 328 (2010) 1689–1699. doi:10.1017/CBO9781107415324.004.

[12] A.-M.A. Willmore, L. Simón-Gracia, K. Toome, P. Paiste, V.R. Kotamraju, T. Mölder, K.N. Sugahara, E. Ruoslahti, G.B. Braun, T. Teesalu, Targeted silver nanoparticles for ratiometric cell phenotyping., Nanoscale. (2015). doi:10.1039/c5nr07928d.

[13] K.N. Sugahara, T. Teesalu, P.P. Karmali, V.R. Kotamraju, L. Agemy, O.M. Girard, D. Hanahan, R.F. Mattrey, E. Ruoslahti, Tissue-Penetrating Delivery of Compounds and Nanoparticles into Tumors, Cancer Cell. 16 (2009) 510–520. doi:10.1016/j.ccr.2009.10.013.

[14] K.N. Sugahara, P. Scodeller, G.B. Braun, T.H. De Mendoza, C.M. Yamazaki, M.D. Kluger, J. Kitayama, E. Alvarez, S.B. Howell, T. Teesalu, E. Ruoslahti, A.M. Lowy, A tumor-penetrating peptide enhances circulation-independent targeting of peritoneal carcinomatosis, J. Control. Release. 212 (2015) 59–69. doi:10.1016/j.jconrel.2015.06.009.

[15] C. Puig-Saus, L.A. Rojas, E. Laborda, A. Figueras, R. Alba, C. Fillat, R. Alemany, iRGD tumor-penetrating peptide-modified oncolytic adenovirus shows enhanced tumor transduction, intratumoral dissemination and antitumor efficacy., Gene Ther. 21 (2014) 767–74. doi:10.1038/gt.2014.52.

[16] K. Wang, X. Zhang, Y. Liu, C. Liu, B. Jiang, Y. Jiang, Tumor penetrability and anti-angiogenesis using iRGD-mediated delivery of doxorubicin-polymer conjugates., Biomaterials. 35 (2014) 8735–47. doi:10.1016/j.biomaterials.2014.06.042.

[17] G. Gu, X. Gao, Q. Hu, T. Kang, Z. Liu, M. Jiang, D. Miao, Q. Song, L. Yao, Y. Tu, Z. Pang, H. Chen, X. Jiang, J. Chen, The influence of the penetrating peptide iRGD on the effect of paclitaxel-loaded MT1-AF7p-conjugated nanoparticles on glioma cells., Biomaterials. 34 (2013) 5138–48. doi:10.1016/j.biomaterials.2013.03.036.

[18] Y. Akashi, T. Oda, Y. Ohara, R. Miyamoto, T. Kurokawa, S. Hashimoto, T. Enomoto, K. Yamada, M. Satake, N. Ohkohchi, Anticancer effects of gemcitabine are enhanced by co-administered iRGD peptide in murine pancreatic cancer models that overexpressed neuropilin-1., Br. J. Cancer. 110 (2014) 1481–7. doi:10.1038/bjc.2014.49.

[19] L. Agemy, D. Friedmann-Morvinski, V.R. Kotamraju, L. Roth, K.N. Sugahara, O.M. Girard, R.F. Mattrey, I.M. Verma, E. Ruoslahti, Targeted nanoparticle enhanced proapoptotic peptide as potential therapy for glioblastoma., Proc. Natl. Acad. Sci. U. S. A. 108 (2011) 17450–5. doi:10.1073/pnas.1114518108.

[20] C. Schmithals, V. Köberle, H. Korkusuz, T. Pleli, B. Kakoschky, E.A. Augusto, A.A. Ibrahim, J.M. Arencibia, V. Vafaizadeh, B. Groner, H.-W. Korf, B. Kronenberger, S. Zeuzem, T.J. Vogl, O. Waidmann, A. Piiper, Improving Drug Penetrability with iRGD Leverages the Therapeutic Response to Sorafenib and Doxorubicin in Hepatocellular Carcinoma., Cancer Res. 75 (2015) 3147–54. doi:10.1158/0008-5472.CAN-15-0395.

[21] H.-B. Pang, G.B. Braun, T. Friman, P. Aza-Blanc, M.E. Ruidiaz, K.N. Sugahara, T. Teesalu, E. Ruoslahti, An endocytosis pathway initiated through neuropilin-1 and regulated by nutrient

availability., Nat. Commun. 5 (2014) 4904. doi:10.1038/ncomms5904.

[22] J. Gaitzsch, X. Huang, B. Voit, Engineering Functional Polymer Capsules toward Smart Nanoreactors., Chem. Rev. 116 (2015) 1053–1093. doi:10.1021/acs.chemrev.5b00241.

[23] G. Battaglia, A.J. Ryan, Bilayers and interdigitation in block copolymer vesicles., J. Am. Chem. Soc. 127 (2005) 8757–64. doi:10.1021/ja050742y.

[24] B.M. Discher, Y.Y. Won, D.S. Ege, J.C. Lee, F.S. Bates, D.E. Discher, D.A. Hammer, Polymersomes: tough vesicles made from diblock copolymers., Science. 284 (1999) 1143–6. http://www.ncbi.nlm.nih.gov/pubmed/10325219 (accessed April 24, 2016).

[25] H. Bermudez, A.K. Brannan, D.A. Hammer, F.S. Bates, D.E. Discher, Molecular Weight Dependence of Polymersome Membrane Structure, Elasticity, and Stability, Macromolecules. 35 (2002) 8203–8208. doi:10.1021/ma020669l.

[26] C. Pegoraro, D. Cecchin, J. Madsen, N. Warren, S.P. Armes, S. MacNeil, A. Lewis, G. Battaglia, Translocation of flexible polymersomes across pores at the nanoscale., Biomater. Sci. 2 (2014) 680–92. doi:10.1039/c3bm60294j.

[27] L. Simon-Gracia, H. Hunt, P.D. Scodeller, J. Gaitzsch, G.B. Braun, A.-M.A. Willmore, E. Ruoslahti, G. Battaglia, T. Teesalu, Paclitaxel-loaded Polymersomes for Enhanced Intraperitoneal Chemotherapy, Mol. Cancer Ther. 15 (2016) 670–680. doi:10.1158/1535-7163.MCT-15-0713-T.

[28] J. Du, Y. Tang, A.L. Lewis, S.P. Armes, pH-sensitive vesicles based on a biocompatible zwitterionic diblock copolymer, J. Am. Chem. Soc. 127 (2005) 17982–17983. doi:10.1021/ja056514l.

[29] H. Lomas, I. Canton, S. MacNeil, J. Du, S.P. Armes, A.J. Ryan, A.L. Lewis, G. Battaglia, Biomimetic pH Sensitive Polymersomes for Efficient DNA Encapsulation and Delivery, Adv. Mater. 19 (2007) 4238–4243. doi:10.1002/adma.200700941.

[30] M. Massignani, C. LoPresti, A. Blanazs, J. Madsen, S.P. Armes, A.L. Lewis, G. Battaglia, Controlling cellular uptake by surface chemistry, size, and surface topology at the nanoscale., Small. 5 (2009) 2424–32. doi:10.1002/smll.200900578.

[31] M. Massignani, I. Canton, T. Sun, V. Hearnden, S. MacNeil, A. Blanazs, S.P. Armes, A. Lewis, G. Battaglia, Enhanced fluorescence imaging of live cells by effective cytosolic delivery of probes, PLoS One. 5 (2010). doi:10.1371/journal.pone.0010459.

[32] J. Meng, F. Guo, H. Xu, W. Liang, C. Wang, X.-D. Yang, O. Lavi, M.M. Gottesman, D. Levy, F.J. Sharom, L.S. Jabr-Milane, L.E. Van Vlerken, S. Yadav, M.M. Amiji, X. Dong, R.J. Mumper, C.P. Wu, S. Ohnuma, S. V. Ambudkar, C.M. Hu, L. Zhang, R. Bonavia, M. M. Inda, W. K. Cavenee, F. B. Furnari, D.C. Hiss, G.A. Gabriels, P.I. Folb, J. Ma, D.J. Waxman, J.H. Lee, A. Nan, Y. Liu, B. Zhang, B. Yan, C.M. Hu, L. Zhang, X.J. Liang, C.Y. Chen, Y.L. Zhao, P. C. Wang, C.M. Hu, S. Aryal, L. Zhang, H. Thomas, H.M. Coley, R. Rezzani, M.F. Phillips, R. Quinlivan, G.D. Pennock, C.H. Choi, Y. Shukla, R. Singh, S. V. Penumathsa, N. Maulik, X. Chang, E. Heene, F. Qiao, P. Nick, E. Sexton, M.Y. Kim, Y. Fang, V.G. DeMarco, M.B. Nicholl, X.X. Wang, F. Quan, Q.P.C. Ma, S. Zhang, L. Yan, K.J. Harrington, A. Albanese, P.S. Tang, W.C. Chan, M.L. Van Slooten, S.H. Kweon, J.H. Song, T.S. Kim, C.E. Soma, C. Dubernet, D. Bentolila, S. Benita, P. Couvreur, D. Belpomme, M.L. Immordino, F. Dosio, L. Cattel, P. Detampel, O.F. Iwuchukwu, S. Nagar, J. V. Jokerst, T. Lobovkina, R.N. Zare, S.S. Gambhir, F. Erogbogbo, Combination Therapy using Co-encapsulated Resveratrol and Paclitaxel in Liposomes for Drug Resistance Reversal in Breast Cancer Cells in vivo, Sci. Rep. 6 (2016) 22390. doi:10.1038/srep22390.

[33] I. Canton, M. Massignani, N. Patikarnmonthon, L. Chierico, J. Robertson, S.A. Renshaw, N.J.

Warren, J.P. Madsen, S.P. Armes, A.L. Lewis, G. Battaglia, Fully synthetic polymer vesicles for intracellular delivery of antibodies in live cells., FASEB J. 27 (2013) 98–108. doi:10.1096/fj.12-212183.

[34] L. Wang, L. Chierico, D. Little, N. Patikarnmonthon, Z. Yang, M. Azzouz, J. Madsen, S.P. Armes, G. Battaglia, Encapsulation of biomacromolecules within polymersomes by electroporation., Angew. Chem. Int. Ed. Engl. 51 (2012) 11122–5. doi:10.1002/anie.201204169.

[35] X. Tian, S. Nyberg, P. S Sharp, J. Madsen, N. Daneshpour, S.P. Armes, J. Berwick, M. Azzouz, P. Shaw, N.J. Abbott, G. Battaglia, LRP-1-mediated intracellular antibody delivery to the Central Nervous System., Sci. Rep. 5 (2015) 11990. doi:10.1038/srep11990.

[36] K. Wayakanon, M.H. Thornhill, C.W.I. Douglas, A.L. Lewis, N.J. Warren, A. Pinnock, S.P. Armes, G. Battaglia, C. Murdoch, Polymersome-mediated intracellular delivery of antibiotics to treat Porphyromonas gingivalis-infected oral epithelial cells., FASEB J. 27 (2013) 4455–65. doi:10.1096/fj.12-225219.

[37] C. Pegoraro, D. Cecchin, L.S. Gracia, N. Warren, J. Madsen, S.P. Armes, A. Lewis, S. MacNeil, G. Battaglia, Enhanced drug delivery to melanoma cells using PMPC-PDPA polymersomes, Cancer Lett. 334 (2013) 328–337. doi:10.1016/j.canlet.2013.02.007.

[38] H.E. Colley, V. Hearnden, M. Avila-Olias, D. Cecchin, I. Canton, J. Madsen, S. MacNeil, N. Warren, K. Hu, J.A. McKeating, S.P. Armes, C. Murdoch, M.H. Thornhill, G. Battaglia, Polymersome-mediated delivery of combination anticancer therapy to head and neck cancer cells: 2D and 3D in vitro evaluation., Mol. Pharm. 11 (2014) 1176–88. doi:10.1021/mp400610b.

[39] L. Chierico, A.S. Joseph, A.L. Lewis, G. Battaglia, Live cell imaging of membrane/cytoskeleton interactions and membrane topology., Sci. Rep. 4 (2014) 6056. doi:10.1038/srep06056.

[40] Y. Wang, A nanoparticle-based strategy for the imaging of a broad range of tumours by nonlinear amplification of microenvironment signals, Nat. Mater. 13 (2013) 1–9. doi:10.1038/nmat3819.

[41] D. Demirgöz, T.O. Pangburn, K.P. Davis, S. Lee, F.S. Bates, E. Kokkoli, PR_b-targeted delivery of tumor necrosis factor-α by polymersomes for the treatment of prostate cancer, Soft Matter. 5 (2009) 2011. doi:10.1039/b814217c.

[42] Z. Pang, L. Feng, R. Hua, J. Chen, H. Gao, S. Pan, X. Jiang, P. Zhang, Lactoferrin-conjugated biodegradable polymersome holding doxorubicin and tetrandrine for chemotherapy of glioma rats., Mol. Pharm. 7 (2010) 1995–2005. doi:10.1021/mp100277h.

[43] Z. Pang, H. Gao, Y. Yu, L. Guo, J. Chen, S. Pan, J. Ren, Z. Wen, X. Jiang, Enhanced intracellular delivery and chemotherapy for glioma rats by transferrin-conjugated biodegradable polymersomes loaded with doxorubicin., Bioconjug. Chem. 22 (2011) 1171–80. doi:10.1021/bc200062q.

[44] A. Koga, K. Aoyagi, T. Imaizumi, M. Miyagi, K. Shirouzu, Comparison between the gastric cancer cell line MKN-45 and the high-potential peritoneal dissemination gastric cancer cell line MKN-45P., Kurume Med. J. 58 (2011) 73–9. http://www.ncbi.nlm.nih.gov/pubmed/22531121 (accessed April 24, 2016).

[45] J.V.M. Weaver, I. Bannister, K.L. Robinson, X. Bories-Azeau, S.P. Armes, M. Smallridge, P. McKenna, Stimulus-Responsive Water-Soluble Polymers Based on 2-Hydroxyethyl Methacrylate, Macromolecules. 37 (2004) 2395–2403. doi:10.1021/ma0356358.

[46] G. Mantovani, F. Lecolley, L. Tao, D.M. Haddleton, J. Clerx, J.J.L.M. Cornelissen, K. Velonia, Design and synthesis of N-maleimido-functionalized hydrophilic polymers via copper-mediated living radical polymerization: a suitable alternative to PEGylation chemistry., J. Am. Chem. Soc.

127 (2005) 2966–73. doi:10.1021/ja0430999.

[47] J. Gaitzsch, M. Delahaye, A. Poma, F. Du Prez, G. Battaglia, Comparison of metal free polymer–dye conjugation strategies in protic solvents, Polym. Chem. (2016). doi:10.1039/C6PY00518G.

[48] C. LoPresti, M. Massignani, C. Fernyhough, A. Blanazs, A.J. Ryan, J. Madsen, N.J. Warren, S.P. Armes, A.L. Lewis, S. Chirasatitsin, A.J. Engler, G. Battaglia, Controlling polymersome surface topology at the nanoscale by membrane confined polymer/polymer phase separation., ACS Nano. 5 (2011) 1775–84. doi:10.1021/nn102455z.

[49] L. Ruiz-Pérez, L. Messager, J. Gaitzsch, A. Joseph, L. Sutto, F.L. Gervasio, G. Battaglia, Molecular engineering of polymersome surface topology., Sci. Adv. 2 (2016) e1500948. doi:10.1126/sciadv.1500948.

[50] L. Paasonen, S. Sharma, G.B. Braun, V.R. Kotamraju, T.D.Y. Chung, Z.-G. She, K.N. Sugahara, M. Yliperttula, B. Wu, M. Pellecchia, E. Ruoslahti, T. Teesalu, New p32/gC1qR Ligands for Targeted Tumor Drug Delivery., Chembiochem. 17 (2016) 570–5. doi:10.1002/cbic.201500564.

[51] P.P. Karmali, V.R. Kotamraju, M. Kastantin, M. Black, D. Missirlis, M. Tirrell, E. Ruoslahti, Targeting of albumin-embedded paclitaxel nanoparticles to tumors., Nanomedicine. 5 (2009) 73–82. doi:10.1016/j.nano.2008.07.007.

[52] D.R. Elias, A. Poloukhtine, V. Popik, A. Tsourkas, Effect of ligand density, receptor density, and nanoparticle size on cell targeting, Nanomedicine Nanotechnology, Biol. Med. 9 (2013) 194–201. doi:10.1016/j.nano.2012.05.015.

[53] T. Teesalu, K.N. Sugahara, E. Ruoslahti, Mapping of vascular ZIP codes by phage display., Methods Enzymol. 503 (2012) 35–56. doi:10.1016/B978-0-12-396962-0.00002-1.

[54] D.K. Armstrong, B. Bundy, L. Wenzel, H.Q. Huang, R. Baergen, S. Lele, L.J. Copeland, J.L. Walker, R.A. Burger, Intraperitoneal cisplatin and paclitaxel in ovarian cancer., N. Engl. J. Med. 354 (2006) 34–43. doi:10.1056/NEJMoa052985.

[55] S.M. Noh, Measurement of peritoneal fluid pH in patiens with non-serosal invasive gastric cancer, Yonsei Med. J. 44 (2003) 45–48. doi:200302045 [pii].

[56] D.K. Armstrong, G.F. Fleming, M. Markman, H.H. Bailey, A phase I trial of intraperitoneal sustained-release paclitaxel microspheres (Paclimer) in recurrent ovarian cancer: a Gynecologic Oncology Group study., Gynecol. Oncol. 103 (2006) 391–6. doi:10.1016/j.ygyno.2006.02.029.

[57] Z. Lu, M. Tsai, D. Lu, J. Wang, M.G. Wientjes, J.L.-S. Au, Tumor-penetrating microparticles for intraperitoneal therapy of ovarian cancer., J. Pharmacol. Exp. Ther. 327 (2008) 673–82. doi:10.1124/jpet.108.140095.

[58] S. Yang, R. Feng, Z.-C. Pan, T. Jiang, Q. Xu, Q. Chen, A Comparison of Intravenous plus Intraperitoneal Chemotherapy with Intravenous Chemotherapy Alone for the Treatment of Gastric Cancer: A Meta-Analysis., Sci. Rep. 5 (2015) 12538. doi:10.1038/srep12538.

FUNDING

This work was supported by the European Union through the European Regional Development Fund

(Project No. 2014-2020.4.01.15-0012), by EMBO Installation grant #2344 (to T. Teesalu), European Research Council starting grant GLIOMADDS from European Regional Development Fund (to T. Teesalu), European Research Council starting grant MEVIC (to G. Battaglia), Wellcome Trust International Fellowship WT095077MA (to T. Teesalu), NCI of NIH grant CA152327 (to E. Ruoslahti), Cancer Center Support Grant CA CA30199 (to E. Ruoslahti), and NCI of NIH grant R01CA167174 (to K. N. Sugahara). J. Gaitzsch was supported by a German Science Foundation Postdoctoral Fellowship.

FIGURES:

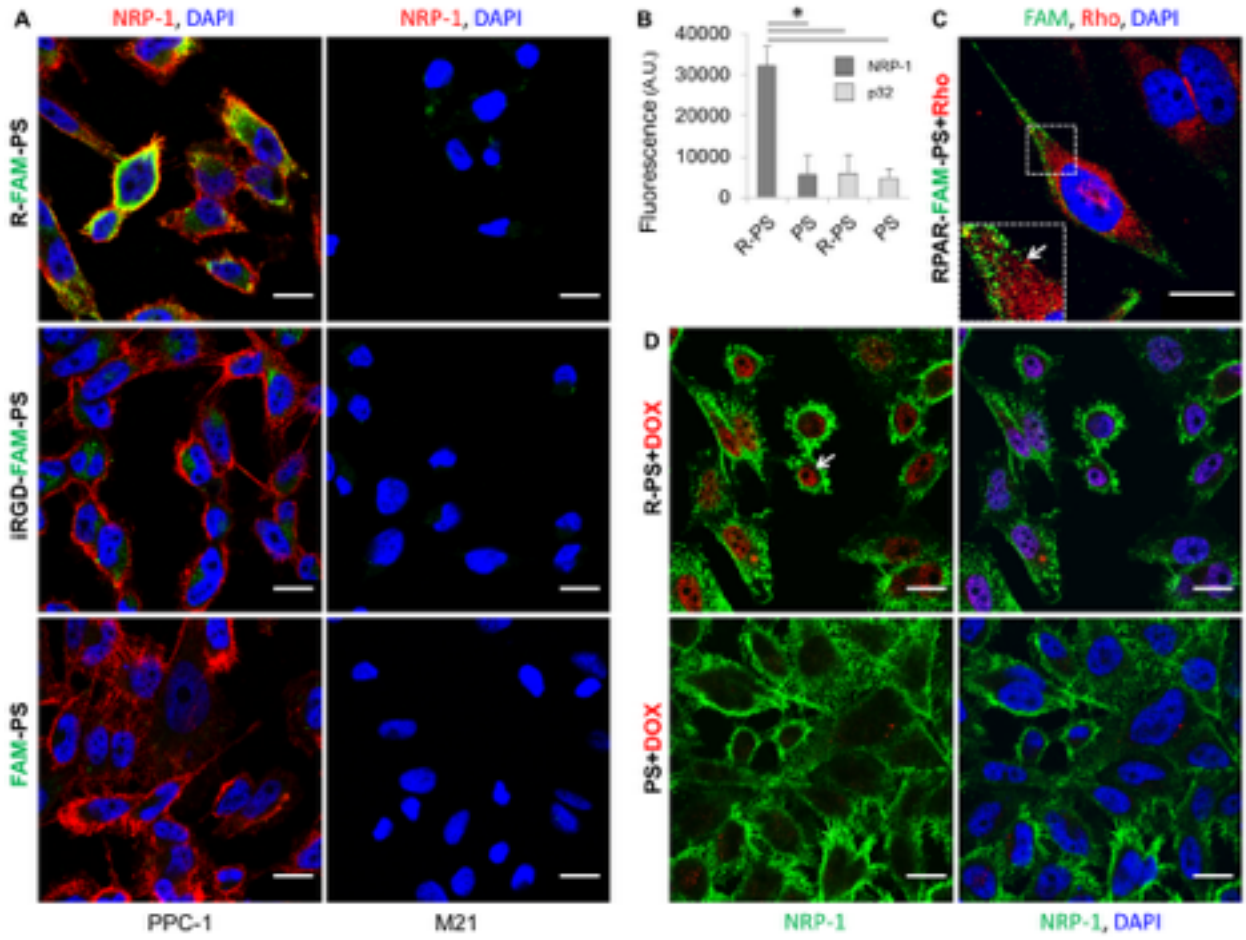

Figure 1

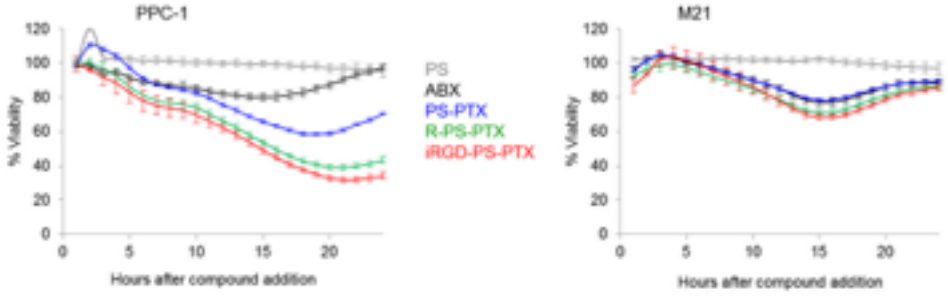

Figure 2

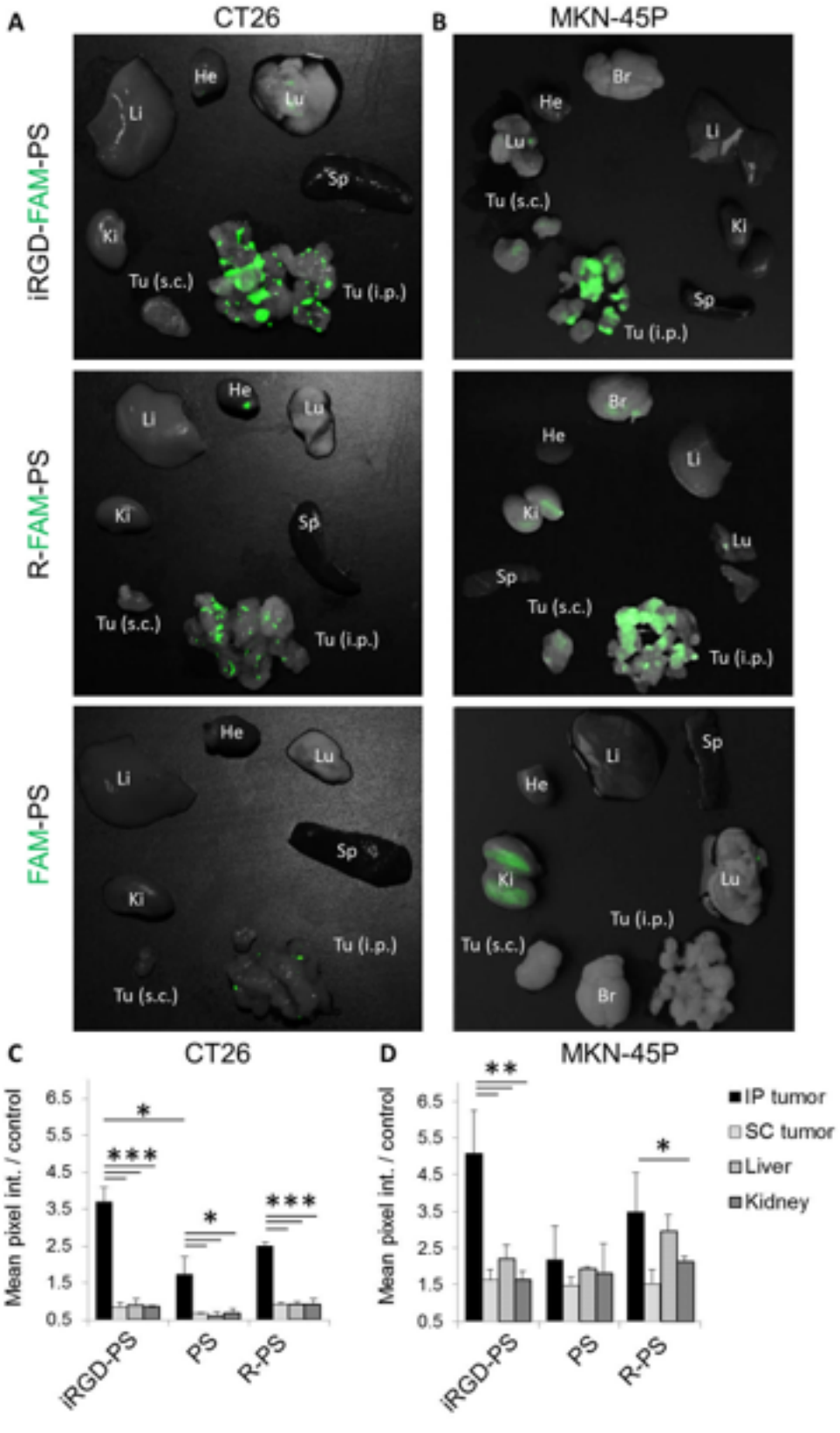
A
CT26
B
MKN-45P
iRGD-FAM-PS
R-FAM-PS
FAM-PS
He
Li
Lu
Sp
Ki
Br
Tu (s.c.)
Tu (i.p.)
C
CT26
D
MKN-45P
Mean pixel int. / control
6.5
5.5
4.5
3.5
2.5
1.5
0.5
*
**
***
iRGD-PS
PS
R-PS
IP tumor
SC tumor
Liver
Kidney

Figure 3

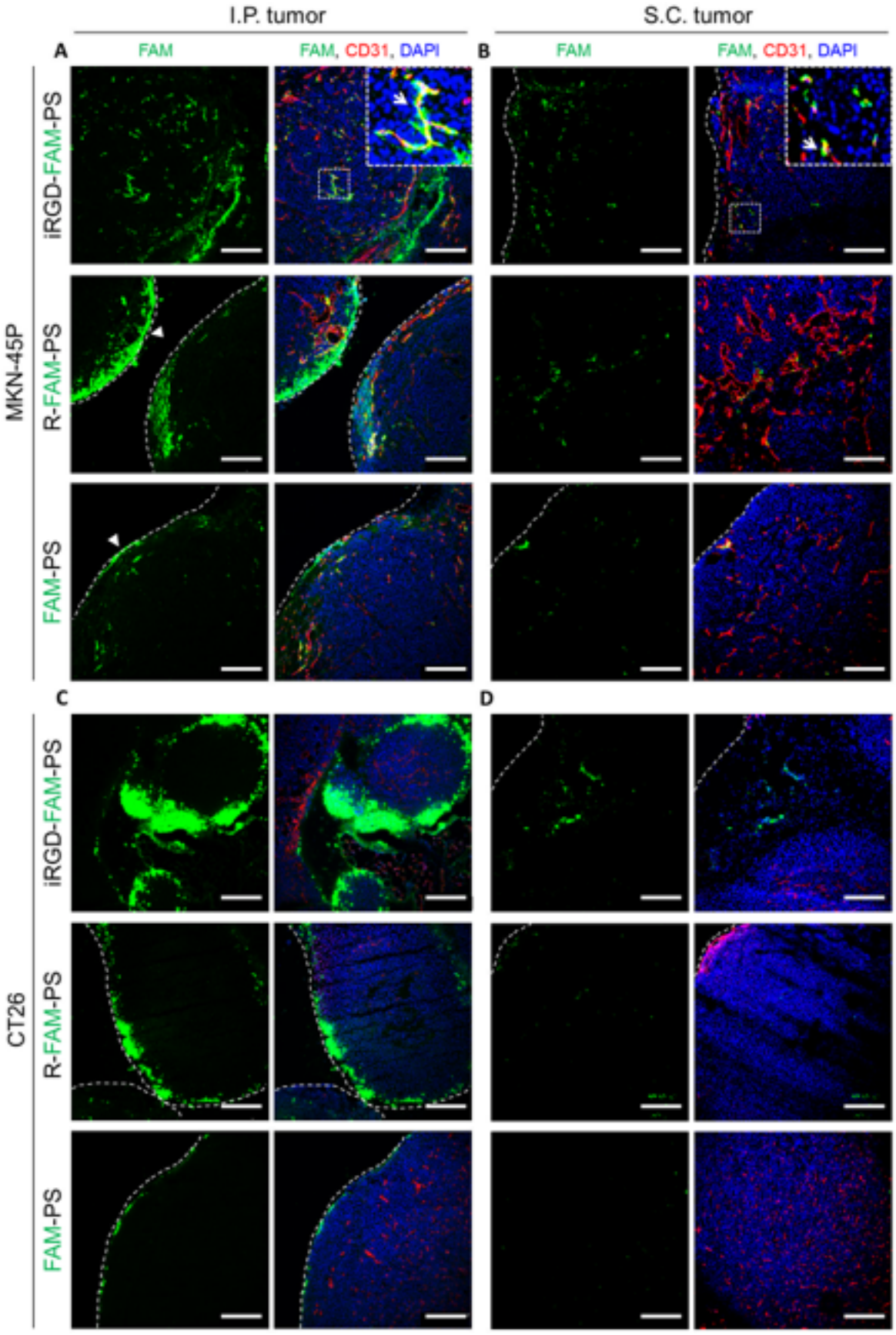
I.P. tumor
S.C. tumor
A
B
C
D
FAM
FAM, CD31, DAPI
MKN-45P
CT26
iRGD-FAM-PS
R-FAM-PS
FAM-PS

Figure 4

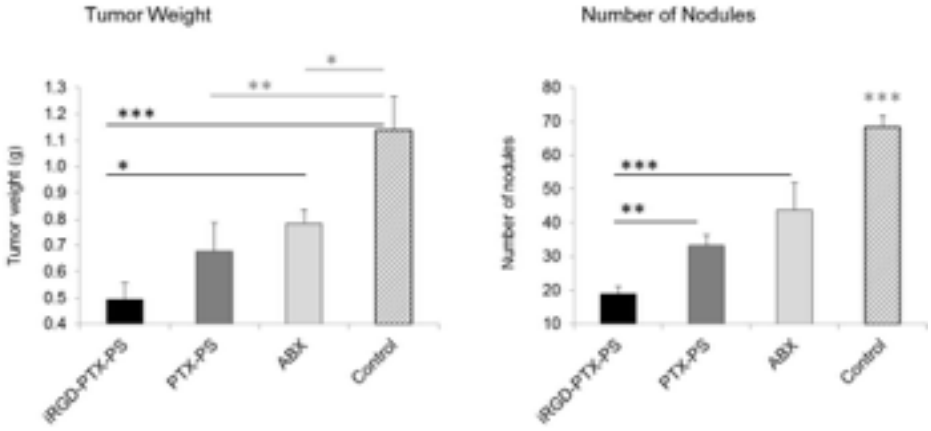

Figure 5

FIGURE CAPTIONS:

Figure 1. Receptor binding, cellular internalization, and cargo release of peptide-targeted polymersomes. (A) Fluorescence confocal imaging of PPC-1 or M21 cells incubated with 0.5 mg/mL of R-FAM-PS, iRGD-FAM-PS or FAM-PS for 1 hour. The cells were stained with DAPI and anti-NRP1. Green: polymersomes; red: NRP-1; blue: DAPI. Scale bars: 20 μm. Representative fields from multiple areas of cultured cells from three independent experiments are shown. **(B)** Binding of R-PS or PS labeled with Rhodamine to recombinant NRP-1 (b1b2 NRP-1) or a control protein, p32, after 1 hour of incubation. For this assay, 0.5 mg/mL of polymersome samples were used. Y axis is the polymersome fluorescence in arbitrary units (A.U.). N = 3; statistical analysis was performed by one-way ANOVA; error bars, mean +SEM, * $p < 0.05$. **(C)** Fluorescence confocal imaging of PPC-1 cells incubated with 0.5 mg/mL of R-FAM-PS loaded with Rho for one hour. The cells were stained with DAPI. Green: polymersomes; red: Rho; blue: DAPI. Scale bar: 20 μm. Representative fields from multiple areas of cultured cells from three independent experiments are shown. **(D)** Fluorescence confocal imaging of PPC-1 cells incubated with 0.5 mg/mL of R-PS or PS loaded with DOX for one hour. The cells were

stained with DAPI. Green: NRP-1; red: DOX; blue: DAPI. Scale bars: 20 μm. Representative fields from multiple areas of cultured cells from three independent experiments are shown.

Figure 2. Effect of paclitaxel-loaded polymersomes on survival of cells with different NRP-1 expression status. Growth rate dynamics of cultured PPC-1 and M21 cells after addition of the R-PS-PTX, iRGD-PS-PTX, or PS-PTX, and ABX at 100 μM PTX concentration, measured using the xCELLigence® real-time cell analyzer that allows continuous quantitative monitoring of attached cells. 100% viability corresponds to untreated cells. Each data point represents the average of three samples. Error bars, mean ±SEM.

Figure 3. In vivo biodistribution of IP-administered polymersomes. (A) Mice bearing dual IP and s.c. MKN-45P or CT26 tumors were IP injected with 0.5 mg of iRGD-FAM-PS, R-FAM-PS, or FAM-PS, and after 4 hours the tumors and organs of interest were excised and fluorescent signal was imaged by Illumatool (Lightools Research, CA). Representative compound fluorescent and bright-field images from three independent experiments are shown. He, heart; Lu, lung; Sp, pleen; Ki, kidney; Li, liver; Br, brain, Tu, tumor. **(B)** Quantification of the fluorescent signal in tumors and control organs by the Image J software. $N \geq 3$ mice; statistical analysis was performed by one-way ANOVA; error bars, mean +SEM; *** $p < 0.001$, ** $p < 0.01$, * $p < 0.05$.

Figure 4. Confocal imaging of polymersomes in tumor tissue. **(A**) Fluorescence confocal images of tissue sections prepared from IP and s.c. MKN-45P and CT26 tumors collected 4 hours after IP injection of polymersomes. Representative images from 3 independent experiments are shown. Green: polymersomes; red: CD31 (blood vessels); blue: DAPI. Scale bars: 250 μm. Arrows point to polymersomes co-localizing with blood vessels; arrowheads point to PS in tumor periphery.

Figure 5. Experimental therapy of tumor mice. Mice bearing disseminated peritoneal MKN-45P tumors were injected IP every other day during two weeks with indicated formulations (cumulative dose

of the treatment: 7 mg PTX/Kg). The tumor weight (weight of large peritoneal tumors combined with small peritoneal tumor nodules) and number of peritoneal tumor nodules after treatment are shown. N = 8 mice in each group; statistical analysis was performed by one-way ANOVA; error bars, mean +SEM; *** $p < 0.001$, ** $p < 0.01$, * $p < 0.05$.